Available online at www.sciencedirect.com
ScienceDirect
International Journal of Mass Spectrometry 265 (2007) 271–280
International Journal of Mass Spectrometry
www.elsevier.com/locate/ijms

# Reduction of ion magnetron motion and space charge using radial electric field modulation

Nathan K. Kaiser, James E. Bruce *

*Department of Chemistry, P.O. Box 644630, Washington State University, Pullman, WA 99164-4630, United States*

Received 2 November 2006; received in revised form 16 February 2007; accepted 21 February 2007
Available online 25 February 2007

**Abstract**

Ions of the same *m*/*z* must remain in phase with each other during the detection time period used for FTICR-MS signal acquisition for optimal performance. The loss of coherence of the ion cloud during detection leads to faster rates of signal decay which results in a decrease in the achievable resolution and mass measurement accuracy with FTICR-MS technology. As the ions spin on their excited cyclotron orbit, many factors contribute to de-phasing of ion motion, such as the presence of radial electric fields and the Coulombic interaction of ion clouds of different mass-to-charge ratios. With the application of Electron Promoted Ion Coherence or EPIC, signal duration can be increased. Since FTICR-MS achieves high performance through measurement of frequency, the ability to observe ions over a longer time period increases the performance of FTICR-MS. Radial electric fields are an unavoidable consequence of applied trapping potentials to confine ion motion parallel to the magnetic field in the ICR cell; however, the presence of radial electric fields also induces magnetron motion. With EPIC it is possible to control the shape of the radial electric fields that the ions experience by changing the number of electrons that are sent through the center of the ICR cell. Furthermore, the electric field shape produced with EPIC can be altered to decrease space charge contributions by increasing the length of the ion oscillation path along the axis of the ICR cell and decrease radial electric field effects, which alter detected ion cyclotron frequencies. Here we report theoretical and experimental results to evaluate and describe the impact of EPIC on the performance of FTICR-MS.


*Keywords:* Magnetron motion; Space charge; FTICR; EPIC

## 1. Introduction

Fourier transform ion cyclotron resonance mass spectrometry FTICR-MS [1] has become an important analytical tool, especially in the analysis of complex mixtures. The capability to provide high resolution, mass measurement accuracy, and sensitivity is important in the area of proteomics [2]. The basis for which FTICR mass spectrometers can offer such high performance is their ability to detect ions for an extended period of time. The mass-to-charge ratio (*m*/*z*) of an ion is determined by measuring the frequency of its excited cyclotron motion in the ICR cell. The longer that the frequency is detected the more accurately the frequency can be determined and the higher the performance of the instrument. The ions are trapped in the detection cell by the Lorentz force (*x*–*y* dimension) and by an electric potential applied to trapping electrodes (*z* dimension). The application of an electrostatic field retains ions in the homogenous region of the magnetic field. However, this electrostatic field also induces magnetron motion and leads to deviations in the observed cyclotron frequency. Magnetron motion changes the observed ion frequency, limits the critical mass that can be stored [3], and causes ion loss and reduced sensitivity. Ideally, the application of trapping potentials will create a three-dimensional axial quadrupolar electrostatic potential, which will result in ion frequency being independent of ion position inside the ICR cell [4].

The stability of an excited ion cloud is critical for detection of image current for an extended period of time [5]. There are many factors which contribute to ion cloud coherence such as ion cloud density [6] and applied trapping potentials [7]. Control of the total ion population trapped in the ICR cell is very critical for the performance of the instrument [8,9]. A trapped population with too few ions leads to a reduction in the signal-to-noise ratio and less stable ion clouds. However, if too many ions are trapped the Coulombic interaction of ion clouds with different mass-to-charge ratios disrupts ion cloud stability, causes ion cloud

* Corresponding author. Tel.: +1 509 335 2116; fax: +1 509 335 8867.
*E-mail address:* james_bruce@wsu.edu (J.E. Bruce).

1387-3806/$ – see front matter © 2007 Elsevier B.V. All rights reserved.
doi:10.1016/j.ijms.2007.02.040

coalescence for closely spaced *m*/*z* species [10], and induces space charge effects. An increase in space charge conditions effectively reduces the observed cyclotron frequency. Due to the presence of quadrupolar trapping fields parallel to the magnetic field, the space charge in the ICR cell is not constant throughout an experiment and results in observed frequency shifts with time [11,12]. Ions which are excited to a large cyclotron orbit can travel a longer distance in the *z*-dimension than if they were located close to the central axis of the cell. As ions traverse their excited cyclotron orbit, they encounter collisions with residual gas molecules, and damp back toward the center of the ICR cell (collisional damping). This causes the ion cyclotron radius to decrease and the ions are funneled back toward the central axis of the ICR cell, where the ions also have a shorter path length in the *z*-dimension. Furthermore, the radial spatial distribution of the ions is decreased with decreased cyclotron radius. The increase in space charge causes the observed cyclotron frequency to shift to lower frequency with time as the ions damp back toward the center of the ICR cell, which causes the *m*/*z* value of the ions to increase to a larger value with time [12].

There has been considerable attention devoted to ICR cell design to improve the performance of FTICR mass spectrometers [13–16]. There are three different types of electrical field shapes that are critical for optimal ICR analysis, including uniform RF electric field for excitation, azimuthal quadrupolar RF electric field for ion axialization, and three-dimensional axial quadrupolar electric field for ion axial confinement [17]. There is usually a compromise between these different electrical field shapes for most ICR cell designs. Solouki et al. [18] suspended a copper wire through the center of the ICR to form electric field potentials that simulate a Kingdon trap [19] which was later described by Gillig et al. [20]. Electrons sent through the center of the ICR cell have previously been used for electron impact ionization, to trap ions in the cell [21], and to perform electron capture dissociation (ECD) [22,23]. The application of an electron beam through the center of the ICR cell during detection has brought interesting results. Easterling and Amster [24] reported that with the presence of a low energy electron beam during detection the transient signals lasted much longer. However, they also reported a current dependent mass shift which in extreme cases approached 10–12 *m*/*z* units. An earlier paper from our group demonstrated that proper tuning of a low energy electron beam, which we call Electron Promoted Ion Coherence or EPIC [25], not only enhanced the time of signal duration but could eliminate frequency shifts and allow acquisition of higher quality spectra. Nikolaev et al. have produced the most accurate computer simulations of ICR motion to date [26], has modeled the effect of an electron beam through the center of the ICR cell, and has shown an increase in ICR signal duration is possible with this configuration [27].

This paper aims to further describe the unique characteristics of EPIC and the basis for an improvement in instrument performance. Here we report that EPIC is a method capable of reducing both radial electric fields from the applied trapping potentials and axial space charge conditions. We present a comparison between theoretical predictions and experimental results of how EPIC affects the electric field shape in the ICR cell. We investigate how the numbers of electrons affect the trapping electric field shape. We also determine how perturbations in the trapping fields affect the mass measurement accuracy.

## 2. Experimental

Electrospray was used as the ionization method. Electrospray solutions consisted of 49/49/2 by volume of water/methanol/acetic acid. All samples (substance p, bradykinin, melittin, and BSA digest) of 10 μM were infused by direct injection with a syringe pump at a rate of 0.4 μL/min. All standard proteins and peptides were purchased from Sigma (St. Louis, MO) and used without further purification. Sequencing grade modified trypsin was purchased from Promega (Madison, WI). A Bruker Daltonics 7T Apex-Q FTICR mass spectrometer (Billerica, MA) was used to acquire the mass spectral data using Xmass version 7.0.6 as the data acquisition software program. Ion accumulation took place in the hexapole ion guide that is external to the magnetic field prior to injection into the ICR cell. Typically the ion accumulation time was set between 0.5 and 1.0 s, but was held constant for all EPIC and non-EPIC comparison spectra. Ions were trapped in an infinity cell [28] using the sidekick technique [29]. The conventional detection technique was modified to perform EPIC experiments. After the ions had been excited to a large cyclotron orbit using a broadband frequency sweep excitation waveform, the electron beam was initiated allowing electrons to traverse the cell. The electron beam was produced with a hollow heated cathode, 3.5 mm i.d., 7.6 mm o.d. The outer diameter of the electron beam entering the ICR cell was determined by a lens which has an i.d. of 6 mm placed between the heated cathode and the back trap plate. The cathode was heated with approximately 1.50 A, the lens was held at ground, and a voltage bias of 0.0 to −1.5 V was placed on the heated cathode to produce an electron beam through the central axis of the ICR cell. At all other times when the cathode was heated there was an applied voltage bias of +10 V. The numbers of electrons that are emitted is determined by the heating current and the applied bias potential. The number of electrons entering the ICR cell is controlled by changing the bias potential since a change in the heating current takes a much longer time to stabilize.

ICR signals were analyzed with ICR-2LS [30]. The time-dependence of the detected frequency was obtained with the sweep [11] module within ICR-2LS, which Fourier transforms consecutive segments of the transient signals. Each segment of the transient signal was Welch apodized, zero-filled three times, and Fourier transformed to obtain a frequency-domain spectrum and allows determination of ion frequency at various points along the transient signal. The number of data points in each segment of the recorded time-domain signal was dependent upon the total data set size; typically parameters for a 128k data set consisted of a segment size of 16,384 points with an advancement of 8192 points.

The resolution and mass accuracy for the broadband experiments were limited by the size of the data sets that could be recorded with the conventional Bruker hardware and software. For extended broadband signal acquisition experiments, the broadband spectra of BSA digest were digitized with a PCI-

6111 National Instruments board (Austin, TX) and recorded on a PC with 512 MB of RAM. The data sets collected were 4 MB at a sample rate of 600,000 Hz. BSA digest spectra were collected after a pulsed gas event to cool the ions followed by a 7 s delay to allow time for the cooling gas to be pumped away.

Simion 7.0 software (SIMION 7.0 3D, version 7.0, D.A. Dahl, Idaho National Engineering Laboratory, Idaho Falls, ID) was used to produce the equipotential field lines, to provide an approximation of the shape of the electric field and the effects of an electron beam through the center of the ICR cell. Electron current was measured on the lens with a current amplifier (Keithley, model 428, Cleveland, OH), with the cathode heated with 1.5 A and various applied voltages.

## 3. Results and discussion

The unperturbed cyclotron frequency is dependent only on the $m/z$ of the ion and the strength of the magnetic field. However, the application of trapping potentials to trap ions in the $z$-axis induces deviations in the observed cyclotron frequency. The magnitude of these deviations depends on the magnitude of the applied trapping potential. The application of an electron beam through the center of the ICR cell during detection has been shown to increase the resolution and the signal-to-noise ratio of FTICR-MS [25]. However, if experimental conditions such as total ion abundance, trap plate potentials, and number of electrons are not carefully controlled, an increase in performance is not observed and can result in large observed frequency shifts. The presence of an electron beam through the center of the ICR cell results in a negative charge along the central axis. This negative charge dramatically alters the shape of the electric field used to confine the ions to a finite space, thus altering the space charge conditions within the cell. Therefore, changes in the measured frequency should be expected. The electric field lines produced within a closed cylindrical cell are shown in Fig. 1a. The segmented trapping electrodes in the infinity cell are used to flatten out the excite potential across the entire cell. Each trapping electrode has the same applied trapping potential with varying RF amplitude applied during the excite. Thus, the shape of the electric field lines produced from the segmented trapping electrodes will be very similar to those generated with a solid trapping electrode. The exact modeling of an electron beam and the affect it will have on the shape of the electric field is not easily solved. However, the presence of electrons will produce a negative potential along the axis of cell. For simplification of modeling efforts, a solid electrode that was biased at a negative potential was used to represent the electron beam. Therefore, the electrode represents a first approximation of the negative potential produced by the electrons and the resulting change in field shape, which is shown in Fig. 1b. The electrons produced

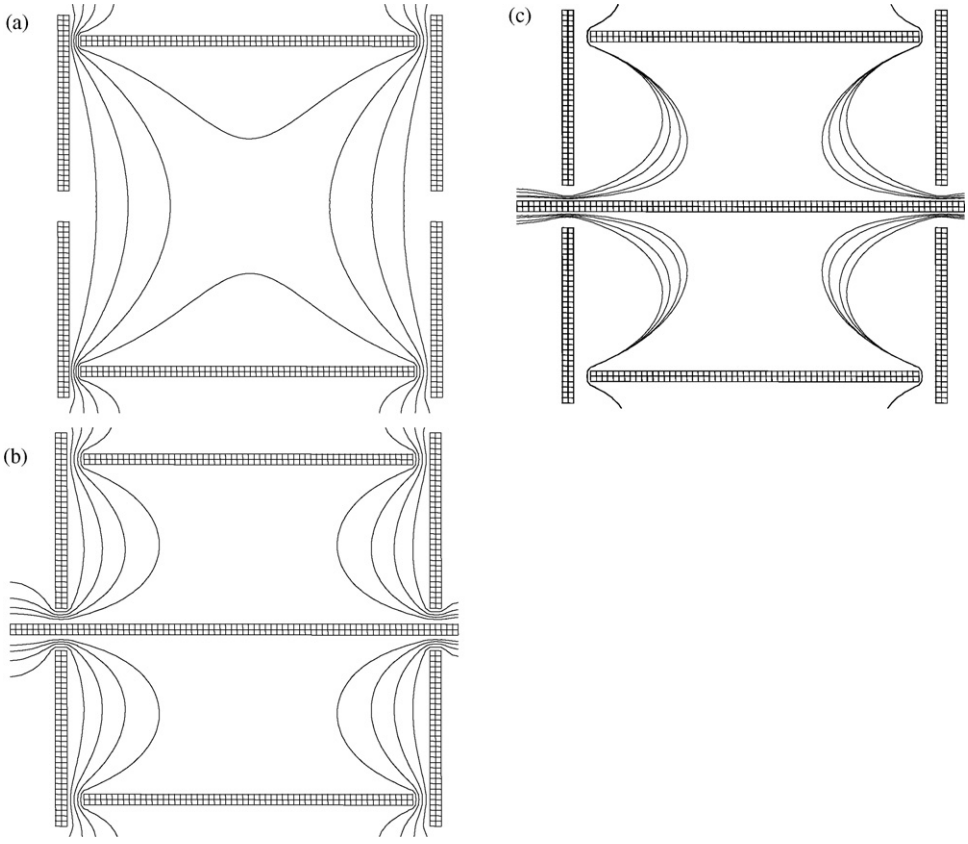


Fig. 1. Simion plot of equipotential contour lines of a closed cylindrical cell with 1.0 V placed on the trapping electrodes. (a) Equipotential contours of 0.8, 0.6, 0.4, 0.2 V are shown, (b) equipotential contours of 0.8, 0.6, 0.4, 0.2 V are shown; an electrode with a −0.5 V potential is placed through the center of the closed cylindrical cell to approximate the affect the electron beam will have on the shape of the trapping potentials, and (c) an overlay of the 0.2 V equipotential contour lines for potentials of −0.01, −0.10, −0.30, and −0.50 V applied to the central electrode.

in the magnetic field will follow the magnetic field lines, thus electrons created on the axis of the ICR cell will remain in a beam on axis through the cell. Any electrons that do scatter in the cell will hit the positive trapping electrodes, thus the negative charge will be kept localized along the $z$-axis of the cell. For the ICR cell with an electron beam through the center, the equipotential contour lines for a given potential do not penetrate as far into the middle of the cell as the unmodified cell (cell with no electron beam). Therefore, ions with the same cyclotron radius and $z$-axis kinetic energy should exhibit a larger range of $z$-axis motion. Fig. 1c shows how the electric field lines are affected by an increase in the number of electrons through the center of the ICR cell. As the potential applied to the central electrode becomes more negative, the electric field lines become closer to the trap plates and the inflection point (point at which radial electric field changes from inward- to outward-directed) is located further from the central axis.

With no electron beam, the electric fields in the cylindrical cell should approximate a three-dimensional axial quadrupolar electrostatic potential. This is important since in this case, cyclotron frequency is independent of cyclotron radius. However, Fig. 2a illustrates the measured cyclotron frequency at different applied excitation voltages and shows that there is a very strong dependence of observed frequency with cyclotron radius. The observed change in frequency can be attributed to alterations in space charge effects at different excited cyclotron radii. Cyclotron radius can affect space charge conditions in two different ways. First, since the trapping potentials approximate a quadrupolar electric field, the $z$-axis oscillation path length decreases as the cyclotron radius gets smaller. Therefore, at smaller cyclotron radii the ions are confined closer axially. Second, at large cyclotron radii, ions with different mass-to-charge ratios will have a greater spatial distribution in the plane perpendicular to the magnetic field. These two effects are detrimental to high performance measurements which require long acquisition time periods, since the measured frequency will change with time. As the ions damp back toward the center of the ICR cell (i.e., exhibit smaller cyclotron radii) the ions become confined to a smaller space increasing the ion density, and thus space charge conditions. This time-based frequency shift behavior may not be observed in all ICR applications, because either the acquisition time period is not long enough or the ions do not stay in a cohesive cloud for a sufficient period of time.

The simulated shape of the electric field lines within the ICR cell with EPIC will no longer form a three-dimensional quadrupolar potential. Therefore, the magnetron frequency of an ion is no longer independent of its radial position in the ICR cell. The observed cyclotron frequency will be dependent upon the radial force exerted by the electric field and thus, the cyclotron radius that the ions exhibit as well as any changes in space charge conditions. This is demonstrated in Fig. 2a which illustrates the observed cyclotron frequency of melittin $(M + 4H)^{4+}$ at different RF excitation voltages with different cathode bias potentials. The observed cyclotron frequencies for different excitation voltages converge at larger cyclotron radii. This indicates that at larger cyclotron radii, the effect from the electron beam is diminished

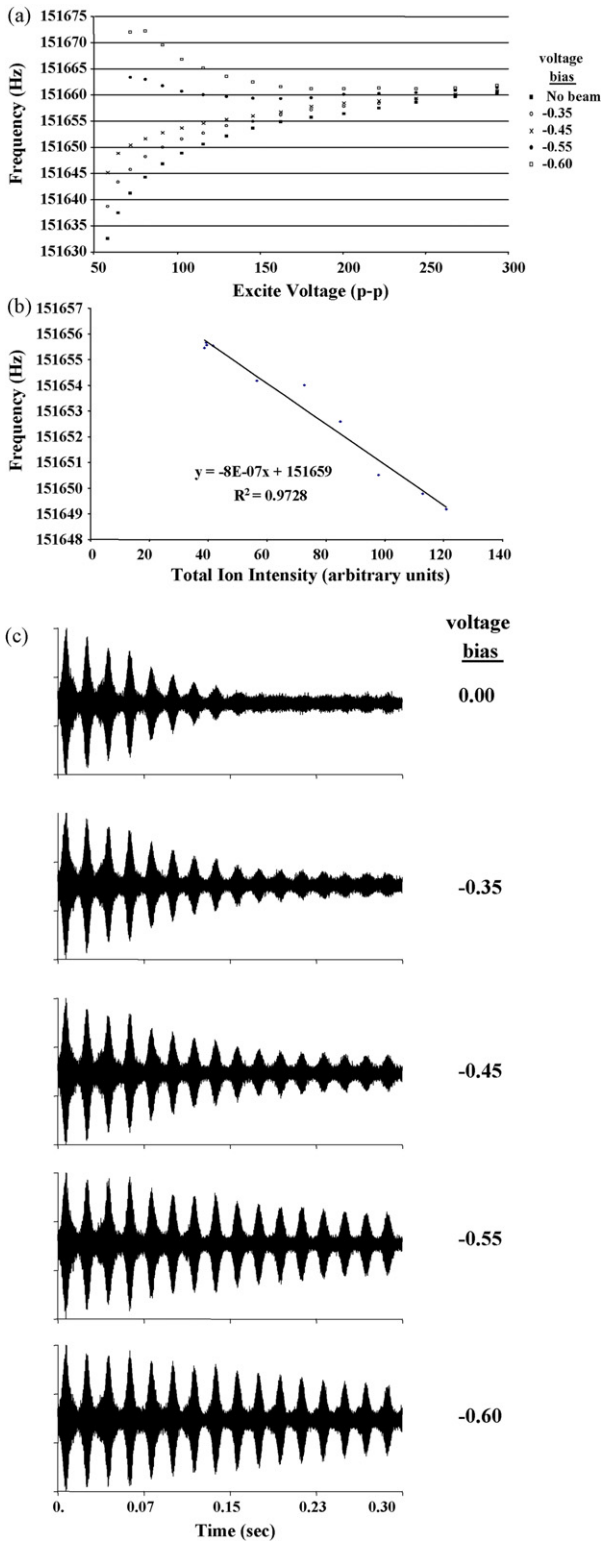


Fig. 2. (a) The measured cyclotron frequency of melittin $(M + 4H)^{4+}$ is plotted at different RF excitation voltages. Experiments were done with different voltage biases applied on the cathode carried out to demonstrate the affect of the number of electrons have on the measured frequency. Each collected spectrum was an average of 10 signal acquisitions and the data set size was 128k. (b) The total ion population in the ICR cell was varied to determine the cyclotron frequency with reduced space charge conditions. (c) The time-domain signal acquired after excitation with voltage of $200V_{p-p}$ is shown for different bias voltages applied to the cathode.

under the beam conditions used for these experiments. However, as the initial cyclotron radius decreases, the ions become closer to the electron beam and the observed differences in cyclotron frequencies increase. This observation can be explained by the electric field shapes in Fig. 1. At greater distances from the central axis, the deviations between the equipotential contour lines in Fig. 1a and b are small and the observed frequencies should be similar. As the distance from the central axis becomes smaller there is a larger deviation in contour lines, which should result in larger differences in observed cyclotron frequencies, and is in agreement with experimentally observed results.

Fig. 2b illustrates the measured cyclotron frequency for different numbers of trapped ions in the cell for the same experimental conditions as in Fig. 2a with no electron beam. This is done to extrapolate the cyclotron frequency that would be observed with no space charge effects. This was determined to be ~151,659 Hz. Any change in the observed cyclotron frequency would then be attributed to a change in the magnetron frequency as shown in Eq. (1) where $\omega_c$ is the unperturbed cyclotron frequency, $\omega_+$ the reduced cyclotron frequency, and $\omega_-$ is the magnetron frequency.

$$\omega_+ = \omega_c - \omega_-. \tag{1}$$

The magnetron frequency is subtracted from the unperturbed cyclotron frequency because the outward direction of the radial fields opposes the force induced by the magnetic field, resulting in a decrease in the observed cyclotron frequency. The space charge-induced frequency shift can be accounted for by introducing an addition term to Eq. (1). McIver and coworkers [31] developed the following equation to account for space charge effect:

$$\omega_{\text{obs}} = \frac{qB}{m} - \frac{2aV}{a^2B} - \frac{q\rho G_{\text{i}}}{\varepsilon_0 B} \tag{2}$$

The first term in the equation describes the unperturbed cyclotron frequency, the second term describes the magnetron frequency in a perfectly quadrupolar static trapping field. While the third term represents the space charge component of the observed frequency, where $q$ is the elementary charge, $\rho$ the ion density, $G_{\text{i}}$ the ion cloud geometry, and $\varepsilon_0$ the permittivity of free space.

The number of electrons that are in the center of the ICR cell is controlled by the bias applied to the heated cathode. The more negative the bias potential the greater the electron current and the larger the negative potential through the center of the ICR cell. Increasing the bias potential will affect the electric field lines similar to what is shown in Fig. 1c. In Fig. 2a, the plot of the data acquired with a cathode bias potential of −0.55 and −0.60 V shows there is an increase in frequency at low excitation voltage, but at higher excitation voltages the frequencies remain constant over a range of excited cyclotron radii. The change in spatial ion distribution perpendicular to the magnetic field is dependent only upon the excitation voltage; therefore, ions should have the same spatial distribution regardless of applied cathode bias. This would lead to an increase in space charge at smaller cyclotron radii which should result in a reduction in observed frequency. However, the reduction in the outward-directed radial field encountered when the electron beam is present in the cell leads to an increase in observed frequency. The two contributions offset each other and result in a frequency that appears more constant at various cyclotron radii. At smaller cyclotron radii the observed frequency increases indicating a larger shift in the magnetron frequency.

The ions excited and detected with the applied cathode bias potential <−0.45 exhibit an increase in frequency for all applied excite potentials, relative to non-EPIC measurements. This is likely because the ions are not excited beyond the inflection point in the equipotential contour lines shown in the SIMION calculations shown in Fig. 1b and c. As the cathode bias potential increases, there is an increase in observed cyclotron frequency for a given excite potential. As the number of electrons increases, the electric field lines are pulled closer to the trap plate which expands the ion path length along the $z$-axis of the ICR cell and decreases the space charge conditions. Therefore, the same ion at a given excite potential within the same ion population will have a different measured cyclotron frequency at different cathode bias potential. As seen in Fig. 1c this change will be more dramatic at lower excite potentials which is also observed experimentally.

In the example shown in Fig. 1b the electric field lines become flat at about half the cell radius, which may not be exact for the applied electron beam. However, with a negative potential through the center of the cell, the positive electric field lines will be drawn toward the center of the trapping electrode resulting in an inflection in the electric field shape. At this inflection point there is no outward-directed radial force to drive magnetron motion. At smaller radii the ion would be located on the interior of the inflection point and there would be an inward-directed radial force. The greater the number of electrons, the greater the negative potential through the center of the cell, and the further from the central axis the inflection point becomes. In comparing −0.55 and −0.60 V bias data in Fig. 2a, both curves reach a minimum frequency as cyclotron radius is increased; however, −0.60 V bias curve reaches a minimum frequency at a larger cyclotron radius, since its expected inflection point is further from the central axis of the cell, as is shown in Fig. 1c. The observed minimum frequency is slightly greater at −0.60 V than the minimum observed frequency for the −0.55 V bias likely due to differences in space charge conditions. There will be a greater axial distribution of the ions at larger bias potentials and greater spatial distribution at larger cyclotron radii. It should be noted that the observed frequencies at a bias potential of −0.50 V should not remain constant over a range of excite potentials because the change in spatial distribution of the ions at different excite amplitudes will alter the space charge conditions.

There are a number of advantages to exciting ions to larger cyclotron radii; there is less space charge contribution, the ions are closer to the detection plates resulting in increased signal. Fig. 2c shows the time-domain signals acquired with the same excitation voltage at different cathode bias potentials. Without any applied bias potential the signal damps quickly and as the cathode bias potential increases the time-domain signal improves. This results in a 1.6-fold increase in the signal-to-noise ratio following comparison of spectra acquired with no electron beam to those acquired with a cathode bias of −0.60 V.

For this example, the improvement in signal-to-noise ratio was limited by the size of the data set acquired, since the signal amplitude is dependent upon the magnitude of the image current and how long it is detected. However, if the post-excitation radius of the ions exceeds ~70% of the cell radius, image current interactions increase and result in a decrease in mass measurement accuracy and detected ion abundances [32–34]. The post-excitation voltage can be approximated by Eq. (3):

$$r_{\text{excite}} = \frac{V_{\text{p–p}}\beta_{\text{dip}}\sqrt{1/\text{sweep rate}}}{2dB_0} \quad (3)$$

where $r_{\text{excite}}$ is the post-excitation radius (m), $V_{\text{p–p}}$ the amplitude of the RF voltage, $\beta_{\text{dip}}$ the dipolar constant (0.9 for infinity cell), the sweep rate was $3.48 \times 10^8$ Hz/s, $B_0$ the magnetic field strength (7 T), and $d$ is the ICR cell diameter (m). Therefore, RF excite voltage of 300 V corresponds to ~57% of the cell radius. However, it should be noted that since the ions are trapped using the sidekick method, the ions are not located directly on the axis of the ICR cell at the beginning of the excite. Therefore, the exact post-excitation radius is not known, although 50–60% of the cell radius is a reasonable approximation.

With the application of EPIC, the radial field can be made flatter at larger radii. Radial electric fields are plotted in Fig. 3 at different ICR cell radii with and without the electron beam. The radial electric fields for a closed cylindrical ICR cell were calculated with SIMION 7.0. The radial electric fields induce magnetron motion. The negative values have an outward-directed value from the central axis of the ICR cell, while the positive values have an inward directing value. Fig. 3 shows that magnetron motion should not be constant as an ion oscillates along the $z$-axis. Generally, the larger the cyclotron radius that an ion exhibits, the larger the deviation in the radial field the ion will experience as the ions oscillate over the same distance along the $z$-axis. These deviations in radial electric field produce deviations in magnetron motion and may lead to de-phasing of the ion cloud. This is especially true of ion populations with a wide distribution of $z$-axis kinetic energies. With the application of the electron beam, it is possible to flatten out the radial field over a set radius, as is shown in the SIMION results. Therefore, as the ion oscillates along the $z$-axis the magnitude of the radial field remains constant.

As the ions spin on their excited cyclotron orbits they encounter collisions with residual neutral molecules in the cell. These collisions cause the cyclotron orbit to decrease with time. Since the frequency of the ion is dependent upon its radial location in the ICR cell, as the ion damps back toward the center of the ICR cell it should experience a shift in frequency. This frequency shift is based on continually decreasing radius with time and should follow the same trend in frequency change as if the ions were excited to different cyclotron radii as shown in Fig. 2a. Fig. 4 illustrates the frequency of bradykinin $(M + 2H)^{2+}$ over time for different excitation voltages with the same voltage bias applied to the cathode. At larger excitation voltages there is an initial decrease in frequency with time indicting that the ions are being excited beyond the inflection point and there is an outward directed radial force (similar to as if no electron beam had been applied). With time, the ions cyclotron radii decrease and they begin to experience change in their magnetron motion at which point the observed cyclotron frequency levels off. As the ions continue to encounter collisions they may pass through the inflection point at which point they begin to feel an inward directing force from the radial fields, where the magnetron motion reverses direction and the observed frequency increases. The frequencies level out at an earlier time point in the detected signals as the excitation voltage decreases, indicating that their initial excited cyclotron radii are closer to the inflection point.

To further demonstrate how the radial fields are affected by the application of EPIC, the frequency of bradykinin $(M + 2H)^{2+}$ is monitored over the acquisition time period at different bias

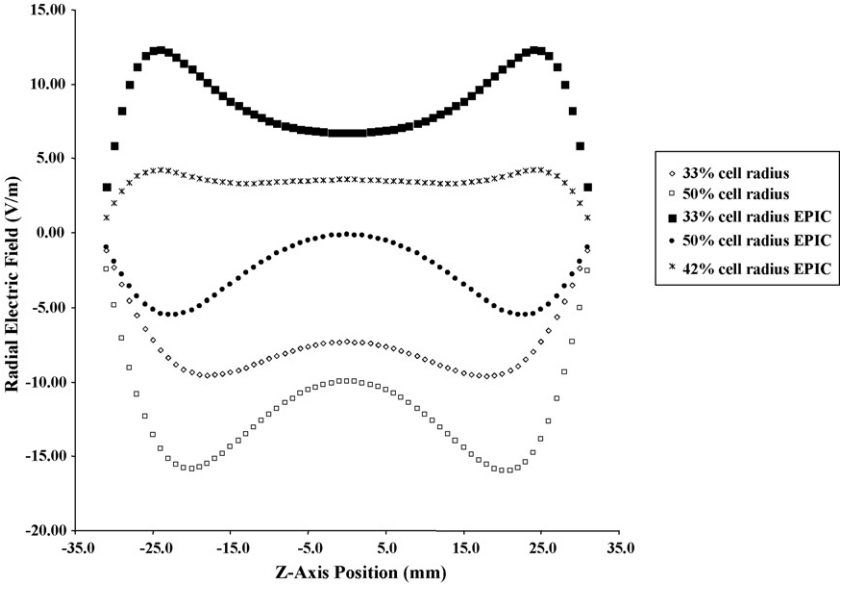


Fig. 3. Radial electric fields are shown at set radii across the $z$-axis of the ICR cell; 1 V applied to the trapping electrodes. The EPIC radial electric fields were constructed with −0.2 V on the central electrode.

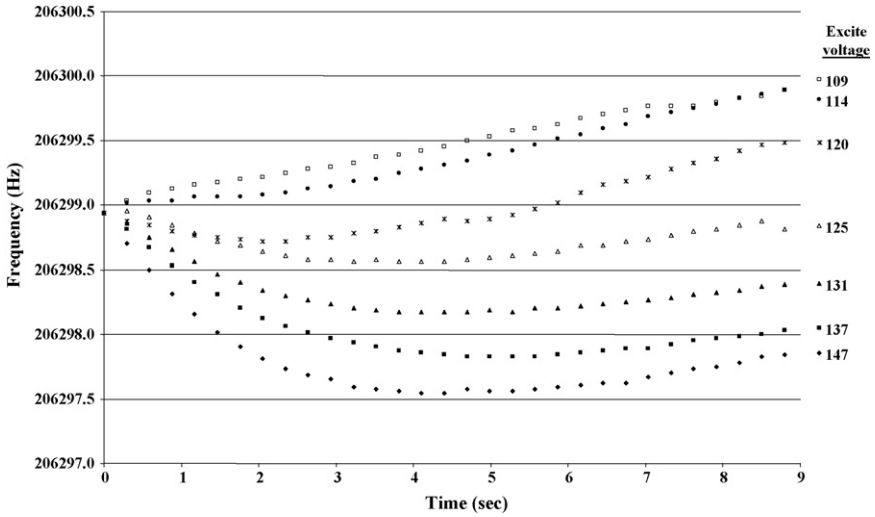


Fig. 4. Segments of time-domain signals of bradykinin $(M + 2H)^{2+}$ collected in heterodyne mode were sampled to monitor the frequency with time while maintaining the same voltage bias to the cathode. Application of various excitation voltages illustrated that the ions pass through the inflection point at different time points based on the initial excited cyclotron radius. The frequencies were normalized to the detected initial frequency from each acquisition to better illustrate the detected frequency shift with time.

potentials to the cathode with the same excitation voltage. The results are shown in Fig. 5. The bias potential applied to the cathode controls the number of electrons that are sent through the center of the ICR cell, and thus the negative charge. This shows the typical effect that the electron beam has on the observed frequency over time. With insufficient electron density at the center of the cell, the frequency will decrease with time in the same manner as if no electron beam was applied. This results from the inflection point in the radial fields being too close to the central axis. If there are too many electrons the frequency increases with time, as the ions are located at a radius which has inward directing radial fields. An important point to note is the general trend that occurs in Fig. 5; the time point at which the observed cyclotron frequency reaches a minimum occurs at an earlier time point with increasing voltage bias. By observing the change in frequency of the ions resultant from the direction and magnitude of the radial force acting on the ions, we can observe the rate the ions are damping back toward the center of the cell. Ideally, the electric fields would be modified to obtain long time-domain signals at larger cyclotron radius where space charge effects are minimal. This can be done by changing the number of electrons and thus, the inversion point of the radial fields and by changing the excitation voltage.

High mass measurement accuracy is a prime attribute of ICR mass spectrometers [35]. The ability to obtain accurate mass measurements is dependent on the ability to detect stable image current for an extended period of time. If the detected frequency is changing with time, it will lead to peak broadening and decrease sensitivity, resolution, and mass measurement accuracy. With the observed frequency shifts that occur with the application of EPIC, we attempted to determine if the mass measurement accuracy is affected by alterations to the radial trapping fields. The mass accuracy was tested with BSA digest peptides which would provide a wide *m*/*z* range of ions to help determine

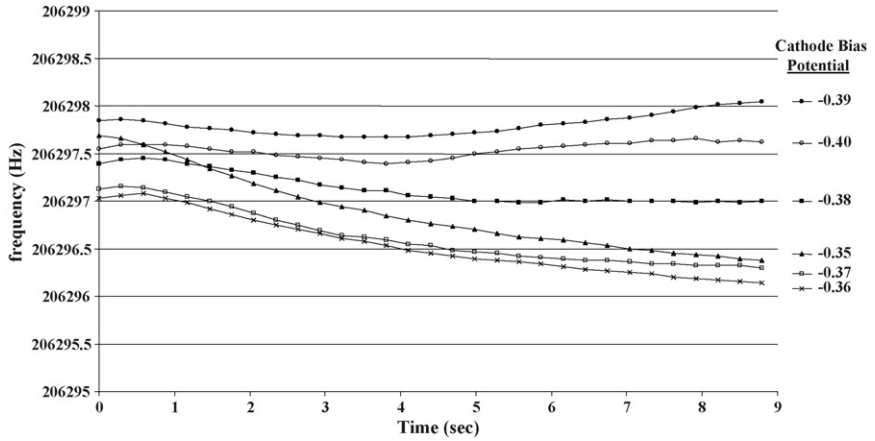


Fig. 5. Segmented FFT analysis of time-domain signals of bradykinin $(M + 2H)^{2+}$ ions. Various cathode bias potentials were applied to demonstrate how the detected frequency changes with time while maintaining the same excited cyclotron radius. At low applied bias potentials the frequency decreases with time. At higher applied bias potentials the frequency increases with time.

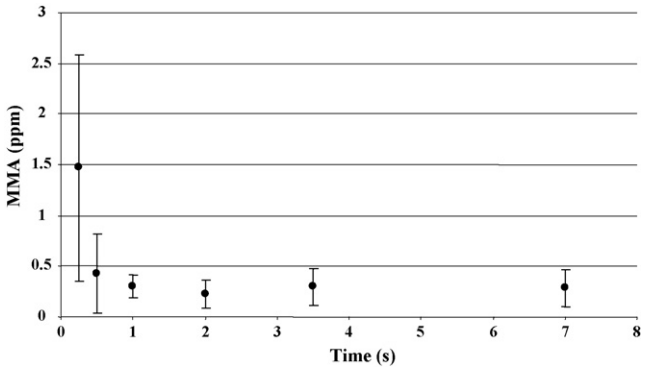


Fig. 6. Broadband spectrum of BSA tryptic digest peptides from a recorded 7 s ICR signal acquisition. The resultant time-domain of a single acquisition period was truncated at time intervals of 0.25, 0.50, 1.0, 2.0, 3.5, 7.0 s. The spectrum was calibrated with five peptides after each truncation. The average mass measurement error of eight other peptides in the spectrum is plotted with time. The error bars show ± one standard deviation.

if there was an *m*/*z* dependence on observed frequency shift. Since the spectra collected in broadband were limited by the data set size available in the conventional Bruker data acquisition hardware, the time-domain signal was simultaneously collected and digitized on a separate computer during signal acquisition. This allowed us to collect much larger data sets to determine if the frequencies of different peptides would change at different rates, thus limiting the improvement of mass measurement accuracy with EPIC. The time-domain signals were truncated at time points of 0.25, 0.50, 1.0, 2.0, 3.5, 7.0 s to observe if the mass measurement accuracy would deviate after extended time periods; no further post-processing was done following truncation. Internal calibration was performed on the same five peptide peaks at each time interval and the mass errors for eight other peptides were calculated. The results of the calibration at each time point are shown in Fig. 6. There is a large increase in mass measurement accuracy within the first second, after which the mass measurement accuracy remains relatively constant. The average absolute mass measurement error for the eight peptides measured was 0.28 ppm after 7.0 s. Therefore, these results show that with proper calibration, EPIC can provide high mass measurement accuracy for a diverse population of different *m*/*z* ions.

De-phasing of the excited ion cloud leads to a loss of ion signal. It is important that the stability of the ion cloud is not compromised with the application of the electron beam due to changes in the shape of the electrostatic trapping field and the radial force acting on the ions. Since the electron beam is turned on after the ions are excited, the ions will experience changes in their frequencies that may disrupt coherent motion of the ion cloud. One way of testing the stability of the ion cloud was to turn the electron beam on-off-on to see if the ion cloud stays together. Fig. 7 shows a graph of the frequencies of substance p $(M+2H)^{2+}$ at various time points for this experiment. The electron beam was turned on initially with −0.43 V bias immediately after excitation, after ∼5 s the electron beam was turned off by changing the bias to 0.00 V, then at ∼8 s the bias to the cathode was switched to −0.50 V. The frequency with time from the switched voltage bias experiment is compared with the frequency with time at constant bias potentials of 0.00, −0.43, and −0.50 V. The frequency in the switched voltage bias experiment matches well with the constant bias potentials. The bias potential of −0.38 V likely resulted in an inflection point in the electric field at a cell radius that is smaller than the post-excitation cyclotron radius. This results in a continual decrease of the observed frequency with time. At −0.50 V bias the frequency is relatively flat with time meaning that the ion cloud is probably close to the inflection point in the electric field lines. In comparing the switched voltage bias to the constant −0.38 V bias we observe a slight deviation in their frequencies. This could be due to the instability of the electron beam, as we discuss below. However, the important point of Fig. 7 is that the stability of the ion cloud is not compromised by turning on and off

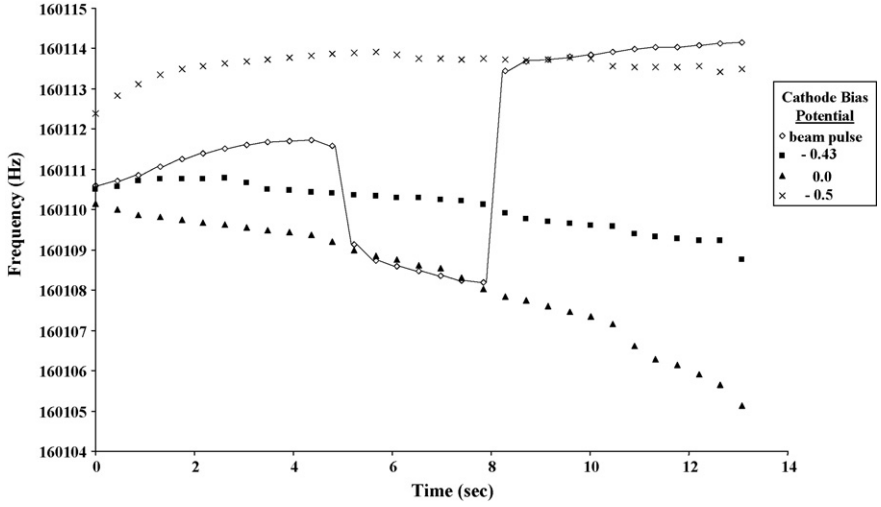


Fig. 7. The effect observed by altering the applied cathode potential during ICR signal acquisition. The frequency of substance p ions was measured throughout the transient signals by segmented FFT analysis. The detected frequency was observed to change abruptly as the electron beam was turned on and off. The detected frequencies obtained at static bias potentials are also shown for comparison.

the electron beam during a single detection event. This illustrates that the number of electrons in the ICR cell can be modulated during the course of a single acquisition without deleterious effects on ion coherence.

One note worth further consideration is the stability of the electron beam. Since the outer diameter of the cathode is larger than the hole in the lens, it is possible to measure a percentage of the electrons emitted from the cathode which hit the lens. There is a slight drift in the electron current over the course of an experiment (1–10 s) which may cause deviations in the frequency of the ion. Fig. 8a shows the electron current which is collected on the lens during typical EPIC experiments at different bias potentials to the cathode. Fig. 8a demonstrates the electron current is not entirely stable with time. Fig. 8b shows the electron current for a single signal acquisition period taken after a number of consecutive signal acquisition periods and the electron current for a single acquisition period after a 5 min delay between experiments. During the delay the cathode was held at +10 V. Both current measurements were taken under identical conditions. The electron current is much higher after some delay period, the exact mechanism for this phenomenon is not currently known. However, the current fluctuations are mostly likely caused by fluctuations in the heating current. However, if multiple spectra are taken after a delay period, the current slowly decreases with each spectrum. The current typically measured on the lens at 1.5 A of heating current and −0.50 V bias on the cathode is ∼3 μA. The electron current drift may limit the ability of high performance measurements since slight changes in the frequency will result in broadening of the peak and less precise determination of the exact cyclotron frequency. The variation in electron current will also make it difficult to signal average a number of high resolution spectra. It would be easier to produce a more accurate and defined negative potential along the central axis of the ICR cell with a solid electrode. The flow of electrons through the cell and unintended changes in electron flow will produce inhomogeneities in the radial electric field. However, the main advantage of the use of the electron beam is that charge is only present in the ICR cell during the detection event.

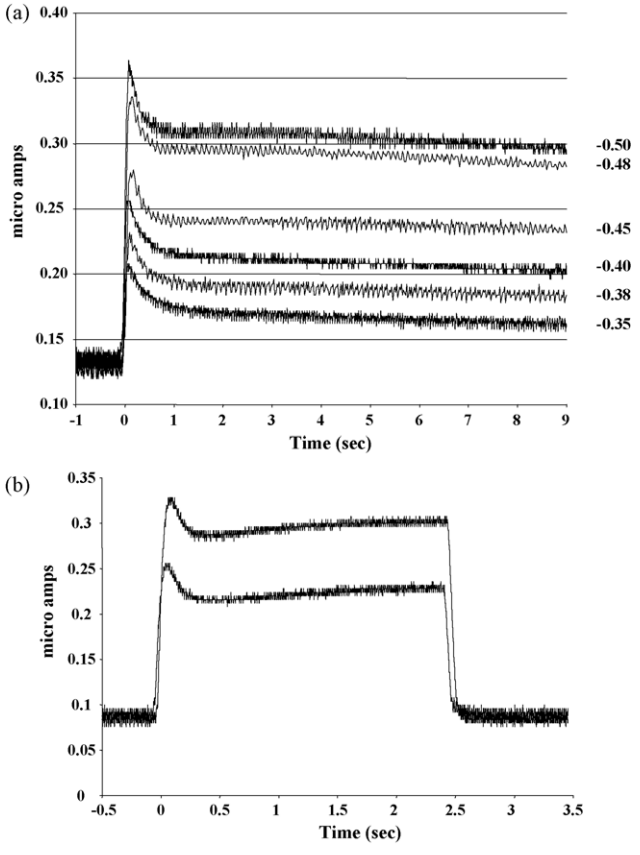


Fig. 8. Time-dependence of electron beam current collected on the lens. (a) The measured electron current resultant from application of various voltage biases to the cathode. The electron current follows the same general drift in current with time. (b) The upper electron current trace was recorded taken after the cathode remained idle for 5 min. The lower current trace was detected immediately after 20 previous signal acquisition periods.

The frequency of an ion is determined by its radial location in the ICR cell as a result of the electron beam. This suggests that modulation of the electron beam could be used to eliminate frequency drift by applying a feedback loop through the bias potential to the cathode. All ions would be excited to the flat part of the electric field at larger cyclotron radii to minimize space charge effects, and the potential to the cathode could be modulated to match the flat part of the electric field with the ions radial position as their cyclotron radius damps back toward the center of the ICR cell.

## 4. Conclusions

The electric field shape can be modulated with the number of electrons present in the center of the ICR cell. Careful control of the number of electrons is needed to increase instrument performance. The application of EPIC forms an inversion point in the equipotential contours which can be determined by monitoring the frequency as a function of excited cyclotron radius. The best performance with EPIC comes when the ions are excited to a cyclotron radius close the inflection point in the radial fields. The cyclotron frequency of an ion can change with time, based on the shape of the electric field and the number of ions present within the ICR cell. The shape of the electric field potentials can be modified to reduce the time based frequency shift, and thus obtain high resolution spectra. The number of electrons being present in the ICR cell is dependent upon the heating current and the applied voltage bias; however, the number of electrons may not be constant from spectrum to spectrum and will limit the performance of this technique if not controlled.

## Acknowledgements

The authors acknowledge helpful discussions with Drs. Jean Futrell and Gökhan Baykut. This material is based upon work supported by the National Science Foundation under Grant No. 0352451; Murdock Charitable Trust; Office of Science (BER), U.S. Department of Energy, Grant No. DE-FG02-04ER63924, and the National Institutes of Health Biotechnology Training Grant.

## References


[1] M.B. Comisarow, A.G. Marshall, Chem. Phys. Lett. 25 (1974) 282.
[2] F. He, M.R. Emmett, K. Hakansson, C.L. Hendrickson, A.G. Marshall, J. Proteome Res. 3 (2004) 61.
[3] M.A. May, P.B. Grosshans, A.G. Marshall, Int. J. Mass Spectrom. Ion Processes 120 (1992) 193.
[4] G.S. Jackson, J.D. Canterbury, S. Guan, A.G. Marshall, J. Am. Soc. Mass Spectrom. 8 (1997) 283.
[5] S.D.H. Shi, C.L. Hendrickson, A.G. Marshall, Proc. Natl. Acad. Sci. U.S.A. 95 (1998) 11532.
[6] A.J. Peurrung, R.T. Kouzes, Phys. Rev. E: Stat. Phys., Plasmas, Fluids, Relat. Interdisciplinary Top. 49 (1994) 4362.
[7] C.L. Holliman, D.L. Rempel, M.L. Gross, Mass Spectrom. Rev. 13 (1994) 105.
[8] M.L. Easterling, T.H. Mize, I.J. Amster, Anal. Chem. 71 (1999) 624.
[9] E.B. Ledford Jr., D.L. Rempel, M.L. Gross, Anal. Chem. 56 (1984) 2744.
[10] D.W. Mitchell, R.D. Smith, Phys. Rev. E: Stat. Phys., Plasmas, Fluids, Relat. Interdisciplinary Top. 52 (1995) 4366.
[11] J.E. Bruce, G.A. Anderson, S.A. Hofstadler, B.E. Winger, R.D. Smith, Rapid Commun. Mass Spectrom. 7 (1993) 700.
[12] S. Guan, M.C. Wahl, A.G. Marshall, Anal. Chem. 65 (1993) 3647.
[13] G.S. Jackson, F.M. White, S. Guan, A.G. Marshall, J. Am. Soc. Mass Spectrom. 10 (1999) 759.
[14] J.E. Bruce, G.A. Anderson, C.-Y. Lin, M. Gorshkov, A.L. Rockwood, R.D. Smith, J. Mass Spectrom. 35 (2000) 85.
[15] C.M. Ostrander, C.R. Arkin, D. Laude, J. Am. Soc. Mass Spectrom. 12 (2001) 30.
[16] S. Guan, A.G. Marshall, Int. J. Mass Spectrom. Ion Processes 146/147 (1995) 261.
[17] V.H. Vartanian, J.S. Anderson, D.A. Laude, Mass Spectrom. Rev. 14 (1995) 1.
[18] T. Solouki, K.J. Gillig, D.H. Russell, Anal. Chem. 66 (1994) 1583.
[19] K.H. Kingdon, Phys. Rev. 21 (1923) 408.
[20] K.J. Gillig, B.K. Bluhm, D.H. Russell, Int. J. Mass Spectrom. Ion Processes 157/158 (1996) 129.
[21] C.L. Hendrickson, F. Hadjarab, D.A. Laude Jr., Int. J. Mass Spectrom. Ion Processes 141 (1995) 161.
[22] N.A. Kruger, R.A. Zubarev, D.M. Horn, F.W. McLafferty, Int. J. Mass Spectrom. 185/186/187 (1999) 787.
[23] F.W. McLafferty, D.M. Horn, K. Breuker, Y. Ge, M.A. Lewis, B. Cerda, R.A. Zubarev, B.K. Carpenter, J. Am. Soc. Mass Spectrom. 12 (2001) 245.
[24] M.L. Easterling, I.J. Amster, 43rd ASMS Conference on Mass Spectrometry and Allied Topics, Atlanta, GA, 1995.
[25] N.K. Kaiser, J.E. Bruce, Anal. Chem. 77 (2005) 5973.
[26] E.N. Nikolaev, A.M. Popov, R.M.A. Heeren, M.S. Sharova, A.V. Pozdneev, K.S. Chingin, I.M. Taban, 53rd ASMS Conference on Mass Spectrometry and Allied topics, San Antonio, TX, 2005.
[27] E.N. Nikolaev, 54th ASMS Conference on Mass Spectrometry and Allied Topics, Seattle, WA, 2006.
[28] P. Caravatti, M. Allemann, Org. Mass Spectrom. 26 (1991) 514.
[29] P. Caravatti, Method and Apparatus for the Accumulation of Ions in a Trap of an Ion Cyclotron Resonance Spectrometer, by Transferring the Kinetic Energy of the Motion Parallel to the Magnetic Field into Directions Perpendicular to the Magnetic Field, US Patent 4,924,089 (1990).
[30] G.A. Anderson, J.E. Bruce, R.D. Smith, ICR-2LS, Richland, WA, 1996.
[31] T.J. Francl, M.G. Sherman, R.L. Hunter, M.J. Locke, W.D. Bowers, R.T. McIver Jr., Int. J. Mass Spectrom. Ion Processes 54 (1983) 189.
[32] M.V. Gorshkov, A.G. Marshall, J. Am. Soc. Mass Spectrom. 4 (1993) 855.
[33] A.M. Hawkridge, A.I. Nepomuceno, S.L. Lovik, C.J. Mason, D.C. Muddiman, Rapid Commun. Mass Spectrom. 19 (2005) 915.
[34] X. Xiang, P.B. Grosshans, A.G. Marshall, Int. J. Mass Spectrom. Ion Processes 125 (1993) 33.
[35] D.R. Goodlett, J.E. Bruce, G.A. Anderson, B. Rist, L. Pasa-Tolic, O. Fiehn, R.D. Smith, R. Aebersold, Anal. Chem. 72 (2000) 1112.